Journal of Materials Chemistry A

ROYAL SOCIETY OF CHEMISTRY

COMMUNICATION

Cite this: *J. Mater. Chem. A*, 2020, **8**, 2369

Received 7th November 2019
Accepted 9th January 2020

DOI: 10.1039/c9ta12244c

rsc.li/materials-a

Giant electrostrictive strain in $(Bi_{0.5}Na_{0.5})TiO_3$–$NaNbO_3$ lead-free relaxor antiferroelectrics featuring temperature and frequency stability

He Qi and Ruzhong Zuo *

Purely electrostrictive materials have shown outstanding advantages for high-precision actuators owing to characteristics such as being hysteresis free, having fast response and low ageing effect and so on. However, their limited achievable strain level, compared with that from piezoelectric materials or antiferroelectric phase-transition materials, and particularly significant temperature sensitivity have been a longstanding obstacle to actual applications in precise actuating or positioning under complex environmental conditions. In this work, a new specially designed lead-free perovskite solid solution was fabricated *via* a conventional solid-state process, which comprises $NaNbO_3$ (NN) with a high-Q_{33} gene and $(Bi_{0.5}Na_{0.5})TiO_3$ (BNT) with an intrinsically high spontaneous polarization gene. A giant purely electrostrictive strain of up to 0.20% varying within less than 10% in a wide temperature range of 25–250 °C and also nearly independent of frequency in the range of 0.01–100 Hz was achieved in the 0.76BNT–0.24NN ceramic, which shows hysteresis-free and linear P–E, S–P^2 and S–E^2 responses within a wide field range at least up to 20 kV mm^{-1}. The excellent electric field-displacement characteristics achieved in this system were basically ascribed to the existence of relaxor antiferroelectric anti-polar nanoregions with an ultrafast discharge (response) speed of ~130 ns, as supported by *in situ* X-ray diffraction and transmission electron microscopy. The achievement of both high electrostrictive strain and excellent stability would make the BNT–NN binary ceramic suitable for large-displacement and high-accuracy actuators where high temperatures are specially required.

Perovskite ceramics with large electrostrain have been widely studied for actuator applications in the last few decades.[1–5] In particular, electrostrictive ceramics have attracted increasing attention for application as inchworm actuators, micro-angle adjusting devices, and bistable optical devices, because the strain induced through the electrostrictive effect offers several unique advantages: excellent displacement accuracy, no remanent strain, reduced ageing effect, and no poling requirement.[6–13] The electrostrictive effect is a basic electromechanical property in dielectrics, all of which can change their dimensions under a bias electric field through the shift of cations away from their natural equilibrium positions. The electric field/polarization induced longitudinal strain S_{33} is expressed by a quadratic term of electric field/longitudinal polarization P_3: $S_{33} = M_{33}E^2 = Q_{33}P_3{}^2$, where M_{33} and Q_{33} are the electrostrictive coefficients.[14] However, the field induced electrostrictive strain is generally quite small, compared with that of the converse piezoelectric effect and the antiferroelectric phase transformation. Hysteresis-free strains of up to 0.1% with the electrostrictive coefficient Q_{33} over 0.02 m^4 C^{-2} in lead-based relaxor ferroelectrics led to systematic studies on electrostrictive ceramics in the 1980s.[6–9] However, it is a known fact that the use of lead oxide would cause serious environmental pollution.[15]

In recent years, a lot of attention has been paid to the development of lead-free electrostrictive ceramics, such as $NaNbO_3$ (NN)-,[12,16] $(Bi_{0.5}Na_{0.5})TiO_3$ (BNT)-[11,12] and $BaTiO_3$ (BT)-[14,17,18] based solid solutions as well as ionic conductors.[19,20] Even though large strains of ~0.2–0.4% with hysteresis-free S–P^2 response were found in these lead-free relaxor ferroelectrics close to the ergodic–nonergodic phase boundary, the large strain hysteresis on S–E curves (>20%) suggests that the contribution of strain is not from the purely electrostrictive effect in these cases.[4,5,12] Purely electrostrictive strains (meaning both hysteresis-free S–P^2 and hysteresis-free S–E response) of ~0.1% can be now achieved in these lead-free ceramics owing to both a large Q_{33} value and a high permittivity value (ε). A usual way to achieve high electrostrictive strains is thus by shifting the temperature of the dielectric maxima (T_m) close to the ambient temperature in relaxor ferroelectrics.[7,12,13] This is basically because Q_{33} is strongly correlated with the chemical species of cations in perovskites, but insensitive to the variation of the phase structure and the ambient temperature.[6,12]As a result, the used temperature range is very important for relaxor ferroelectrics having high electrostrictive strains owing to seriously temperature dependent permittivity. Antiferroelectrics have also shown excellent electromechanical behavior as well as

Institute of Electro Ceramics & Devices, School of Materials Science and Engineering, Hefei University of Technology, Hefei, 230009, P. R. China. E-mail: piezolab@hfut.edu.cn

good temperature stability.[21–23] However, extremely large strain hysteresis is usually accompanied by reversible antiferroelectric–ferroelectric phase transition above a critical field (E_{A-F}).[24] The interesting thing is that a nearly linear polarization-field response corresponding to an almost purely electrostrictive effect can be observed as the applied field is below E_{A-F}. In addition, the introduction of random field into antiferroelectrics by adjusting dielectric relaxation behavior was reported to increase E_{A-F} and enhance dielectric response at the same time, enabling desirable electrostrictive behavior in a wide field range (*i.e.*, higher electric field) below E_{A-F} in so-called relaxor antiferroelectrics. Based on similar structural features,[22] frequency and temperature insensitive energy-storage properties were also observed in BNT–NN binary solid solutions according to the equation $S_{33} = Q_{33}\varepsilon_{33}{}^2E^2$ and the recoverable energy-storage density $W_{rec} = \varepsilon_r\varepsilon_0E^2/2$.

Theoretical analysis[12,25] indicated that a strong ionic bond is of great benefit to the Q_{33} value but deleterious to the saturation polarization P_3, compared with a covalent bond. Therefore, large $Q_{33} \sim 0.046$ m^4 C^{-2} and low $P_3 \sim 20$ μC cm^{-2} were generated in NN-based ceramics owing to the strong ionic behavior of Na^+ ions. Relatively low $Q_{33} \sim 0.022$ m^4 C^{-2} but large $P_3 \sim 40$ μC cm^{-2} was found in BNT-based ceramics owing to the hybridization of Bi 6s orbitals with O 2p orbitals. In this work, solid solutions between ferroelectric BNT and antiferroelectric NN were specially designed. In addition, NN is an effective and frequently used temperature stabilizer in perovskite capacitors.[26,27] As a consequence, temperature and frequency insensitive giant electrostrictive strains were expected in BNT–NN lead-free relaxor antiferroelectrics.

$(1-x)(Bi_{0.5}Na_{0.5})TiO_3$–$x$NaNbO$_3$ ($(1-x)$BNT–xNN) ceramics with $x = 0$–0.24 were prepared by a conventional solid-state process using the standard mixed oxide route with highly pure raw materials Na_2CO_3, Nb_2O_5, Bi_2O_3 and TiO_2. The powders were mixed thoroughly in ethanol using zirconia balls for 12 h in stoichiometric amounts. The mixture was ball-milled again for 24 h after calcination at 850 °C for 5 h and then pressed into disk samples with a diameter of 10 mm under 100 MPa using polyvinyl alcohol as a binder. The disk samples were sintered at 1150–1200 °C for 2 h in air after burning out the binder at 550 °C for 4 h. Silver electrodes were fired on both sides of the samples at 550 °C for 30 min.

Dielectric properties as a function of temperature and frequency were measured with an LCR meter (Agilent E4980A, Santa Clara, CA) and broad-frequency dielectric spectrometer (Concept 80, Novocontrol Inc, Germany). The domain morphology observation and selected area electron diffraction (SAED) were performed on a field-emission transmission electron microscope (FE-TEM, JEM-2100F, JEOL, Japan) operated at 200 kV. A ferroelectric testing system (Precision Multiferroic, Radiant Technologies Inc., Albuquerque, NM) connected with a laser interferometric vibrometer (SP-S 120, SIOS Meβtechnik GmbH, Germany) was used to measure unipolar and bipolar polarization *vs.* electric field (*P*–*E*) hysteresis loops and strain *vs.* electric field (*S*–*E*) curves. The energy release properties of ceramic capacitors were investigated with a commercial charge–discharge platform (CFD-001, Gogo Instruments Technology, Shanghai, China) with a certain discharge resistance, inductance and capacitance (RLC) load circuit. Temperature dependent XRD measurements were performed with Cu Kα radiation under acceleration conditions of 40 kV and 30 mA (D/Max

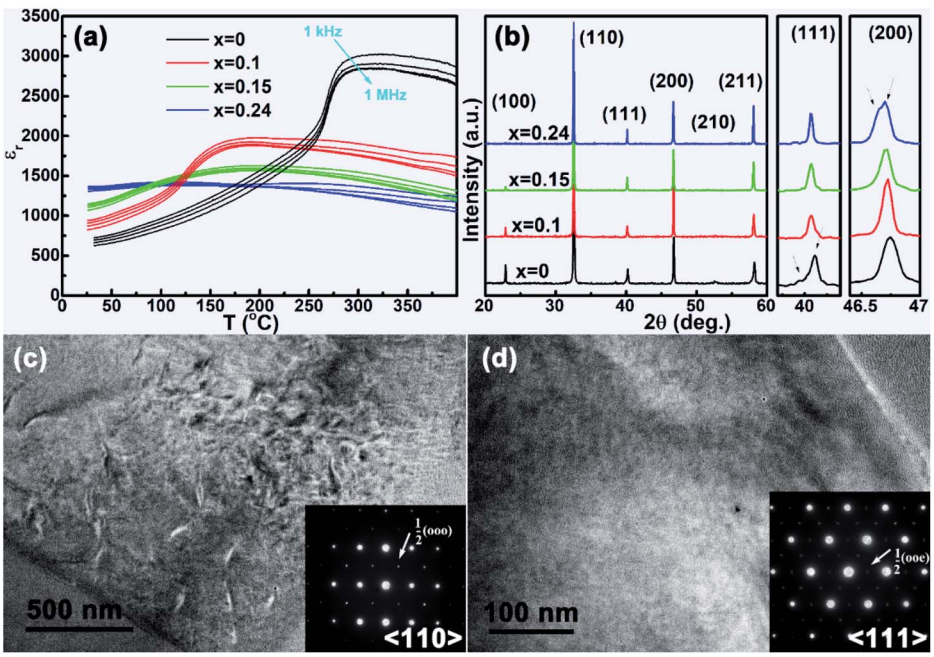

Fig. 1 (a) Dielectric permittivity ε_r with changing temperature and frequency for a few $(1-x)$BNT–xNN ceramics; (b) room temperature XRD patterns and enlarged (111) and (200) diffraction peaks for $(1-x)$BNT–xNN ceramics after the deduction of backgrounds and Cu Kα2 peaks; bright-field image and SAED patterns for (c) $x = 0$ and (d) $x = 0.24$ samples at room temperature.

2500V; Rigaku, Tokyo, Japan). Rietveld refinements were performed by using the GSAS program.

The temperature dependence of the dielectric permittivity of $(1-x)$BNT–xNN ceramics at different frequencies is shown in Fig. 1(a). The T_m value obviously decreases with the addition of NN. Simultaneously, the peak permittivity at T_m is deeply suppressed, leading to much more flat ε–T curves with the substitution of NN for BNT. Meanwhile, obviously enhanced room-temperature dielectric permittivity can be found with increasing the NN content. Nearly a horizontal ε–T line with a large dielectric constant of $\varepsilon_r \sim 1450$ was obtained at room temperature for the $x = 0.24$ ceramic, showing large potential for temperature stable capacitor applications.

A rhombohedral phase can be identified for pure BNT according to the double (111) diffraction peaks and single (200) diffraction peak, as shown in Fig. 1(b). With the addition of NN up to $x = 0.1$ and 0.15, the (111) diffraction peaks gradually merged together, indicating the formation of polar nanoregions within a cubic matrix (relaxor ferroelectrics). However, when $x = 0.24$, the (200) diffraction peaks were split into two peaks in addition to the existing single (111) peak, illustrating the appearance of the tetragonal antiferroelectric phase. Therefore, the addition of NN into BNT induces the phase transformation from normal ferroelectric ($x = 0$), to relaxor ferroelectric ($x = 0.1$ and $x = 0.15$) and finally to tetragonal (relaxor) antiferroelectric ($x = 0.24$). Fig. 1(c) and (d) show TEM bright field images and SAED patterns of $x = 0$ and $x = 0.24$ ceramics, respectively, revealing the change in the domain morphology with the substitution of NN for BNT. Single-phase BNT at $x = 0$ has an irregular or dirty domain morphology, but obvious micro-domains related to long range ordered ferroelectric states can also be observed. The 1/2{*ooo*}-type superlattice spots were observed in the $x = 0$ sample, which are indicative of the ferroelectric *R*3*c* phase. With the addition of 24 mol% NN, faint-contrast anti-polar nanoregions (as defined in the same way for polar nanoregions in relaxor ferroelectrics,[28,29] and in which anti-polar stands for anti-parallel polar vectors in relaxor antiferroelectrics) become dominant. In addition, 1/2{*ooe*}-type

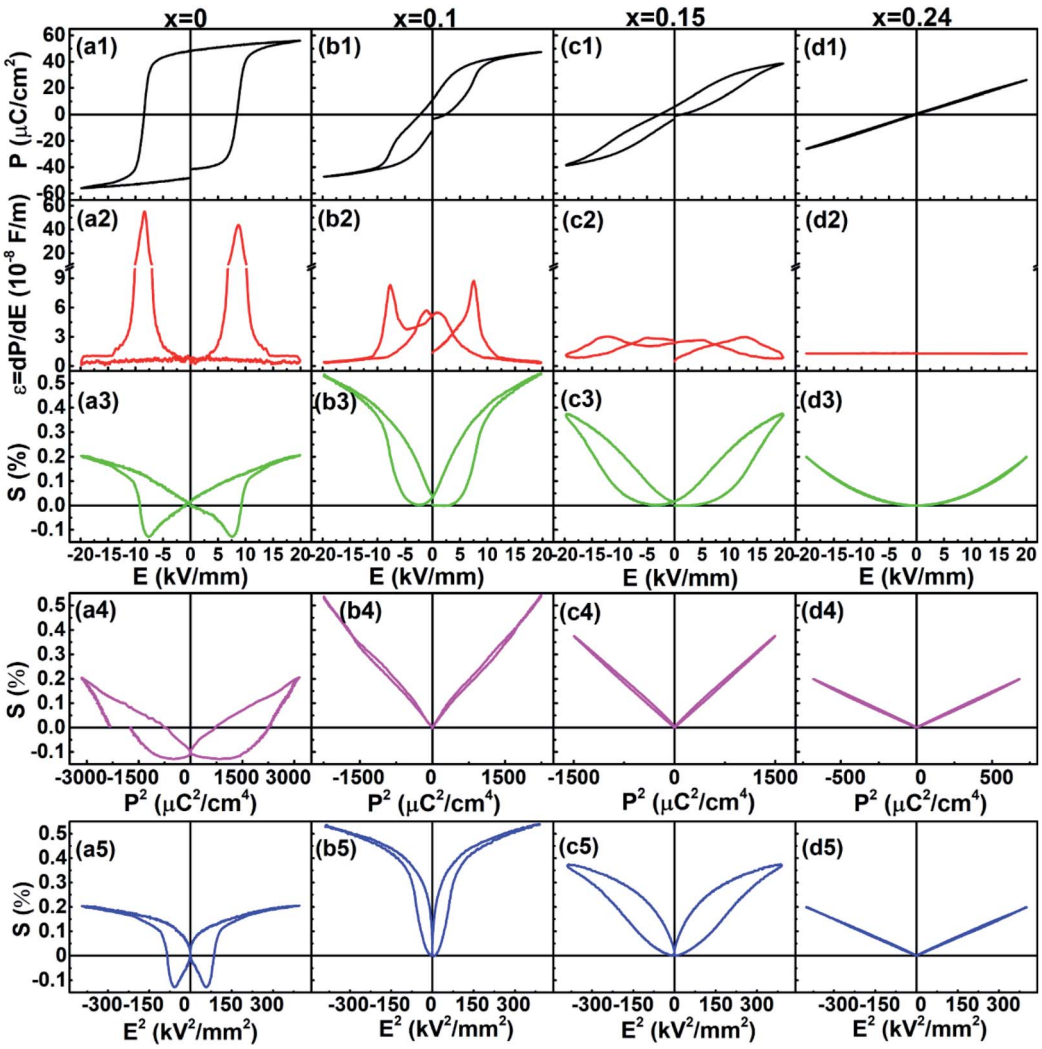

Fig. 2 Room temperature (a1)–(d1) P–E hysteresis loops, (a2)–(d2) the corresponding ε–E curves, (a3)–(d3) bipolar S–E curves, (a4)–(d4) S–P^2 curves and (a5)–(d5) S–E^2 curves measured at 10 Hz for $(1-x)$BNT–xNN ceramics: (a) $x = 0$, (b) $x = 0.1$, (c) $x = 0.15$ and (d) $x = 0.24$.

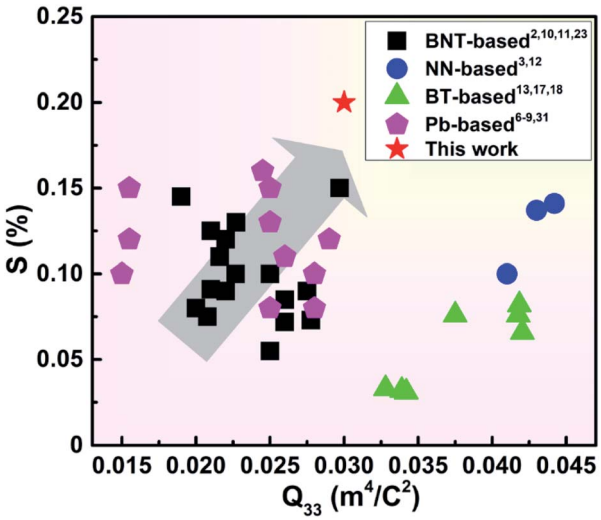

Fig. 3 A comparison of Q_{33} and electrostrictive strains among various types of perovskite ceramics.

superlattice spots related to characteristics of the antiferroelectric *P4bm* phase were found in the SAED patterns of the $x = 0.24$ sample. These results indicate that the addition of NN has a significant impact on the domain structure in the BNT–NN lead-free system, leading to an evolution from the ferroelectric to relaxor antiferroelectric phase.

Fig. 2 shows *P*–*E* hysteresis loops and corresponding ε–*E* curves ($\varepsilon = dP/dE$), *S*–*E* curves and corresponding S–P^2 and S–E^2 curves for various $(1 - x)$BNT–xNN samples. All the studied ceramics show well reproducible high-field responses due to their high density and low losses. A saturated hysteretic *P*–*E* loop was obtained for the BNT ($x = 0$) ceramic, which is a typical feature of normal ferroelectrics. A sharp polarization current peak related to the domain reorientation can be seen in the ε–*E* curves around the coercive field E_C. A typical butterfly-shaped *S*–*E* curve was achieved in the BNT ceramic. As a result, obviously nonlinear and hysteretic relations could be found in the S–P^2 and S–E^2 curves under lower electric fields, which should be related to the irreversible domain switching. The domains can be clamped and the influence of domain switching will be eliminated under a strong electric field, resulting in a hysteresis-free part in S–E^2 curves. With increasing the NN content, a pinched *P*–*E* loop and a dual-peak ε–*E* curve were detected for the specimen of $x = 0.1$, which is a typical feature of relaxor ferroelectrics close to the ergodic and nonergodic phase boundary. A significantly enhanced reversible strain of ~0.54% but with a large hysteresis was generated for the composition of $x = 0.1$. Even though a nearly linear S–P^2 curve can be detected in this ceramic owing to its non-polar nature, the process of field induced relaxor ferroelectric to long-range ordered ferroelectric phase transition instead of pure electrostriction causes an obvious nonlinearity in S–E^2 curves. When $x = 0.15$, *P*–*E* and *S*–*E* loops become slimmer as a result of the increase of the dynamics of the polar nanoregions in relaxor ferroelectrics. With further increasing the NN content up to $x = 0.24$, a strong ergodicity corresponding to anti-polar nanoregions was generated in the composition of $x = 0.24$, leading to hysteresis-free polarization and strain responses to the external electric field

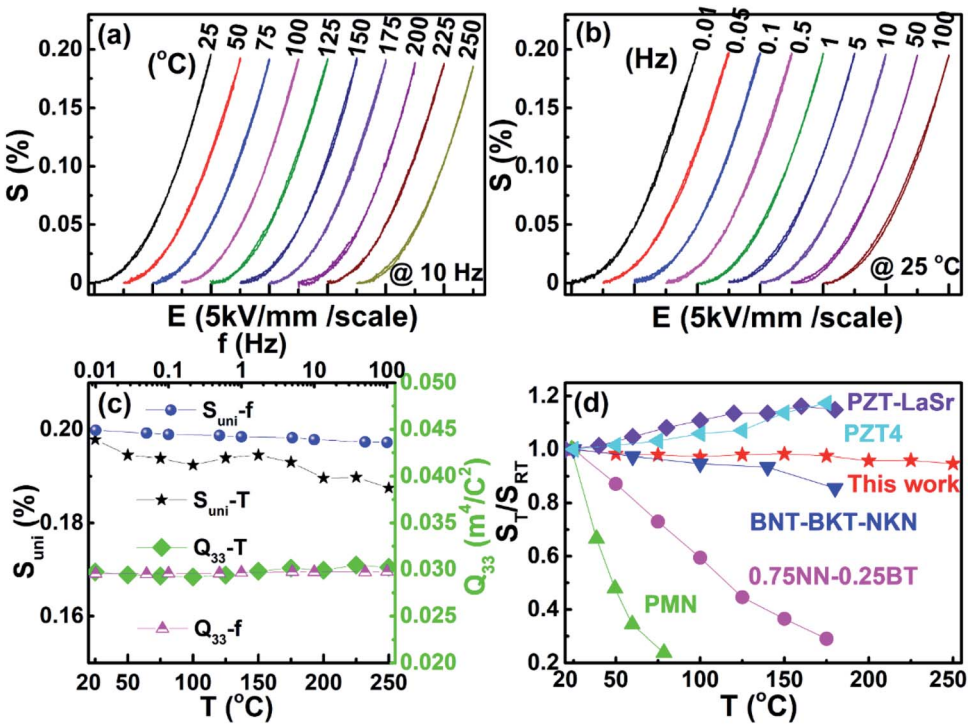

Fig. 4 Unipolar strain curves of the 0.76BNT–0.24NN ceramic measured at various (a) temperatures and (b) frequencies; (c) temperature and frequency dependent S_{uni} and Q_{33} for the 0.76BNT–0.24NN ceramic; (d) temperature dependence of normalized strain S_T/S_{RT} for various perovskite ceramics.

due to a large enough local random field. That is to say, a linear polarization response and a parabolic strain response under 20 kV mm^{-1} indicate a typical feature for nonpolar ceramics with a purely electrostrictive effect. The linear polarization response can also be confirmed by field independent dielectric permittivity during electric cycling in Fig. 2(d2). A giant pure electrostrictive stain of up to 0.20% was obtained in the $x = 0.24$ ceramic, together with a linear S–P^2 curve with the electrostrictive coefficient $Q_{33} = S/P^2 \sim 0.030$ m^4 C^{-2} and a linear S–E^2 curve with the electrostrictive coefficient $M_{33} = S/E^2 \sim 4.9 \times 10^{-18}$ m^2 V^{-2}. The M_{33} of this studied sample is much larger than that of the materials with low dielectric permittivity (<50) and comparable to that of other relaxor ferroelectrics and ionic-conductive electrostrictors.[19,20] A large electrostrictive stress $\sigma \sim$ 200 MPa ($=YM_{33}E^2$, Y is Young's modulus and ~100 GPa for BNT-based ceramics[19,30]) can be calculated for the strain-free $x = 0.24$ ceramic under 20 kV mm^{-1}. Both Q_{33} and M_{33} remain constant within a quite wide field range at least up to 20 kV mm^{-1}. A comparison of Q_{33} and electrostrictive strain (hysteresis free) between various reported ceramics is shown in Fig. 3.[2,3,6–13,17,18,23,31] Owing to the large-Q_{33} gene of NN and the large spontaneous polarization gene of BNT, a moderate Q_{33} as well as a large electrostrictive strain was achieved in BNT–NN ceramics. The achievable hysteresis-free parabolic strain in this work is very attractive among some perovskite ceramics because of significantly increased E_{A-F} values in the relaxor antiferroelectric composition with $x = 0.24$. Comparatively speaking, the electrostrictive values of BNT and Pb-based ceramics are mainly restricted by their relatively low Q_{33} values, and insufficient applied electric fields above which obvious dielectric nonlinearity starts to appear owing to the domain wall motion and subsequent orientation, such that significant strain hysteresis can be observed and M_{33} is not a constant with electric field.[4,5,24] Even though large $Q_{33} > 0.04$ m^4 C^{-2} can be obtained in BT and NN-based lead-free ceramics, the applied electric field should be limited because of nonlinear dielectric response at higher fields,[12,13] leading to a relatively low saturation polarization as well as small electrostrictive strain.

The unipolar S–E curves measured in the temperature range of 25–250 °C for 0.76BNT–0.24NN ceramics are shown in Fig. 4(a). As known, the dynamics increases and the size decreases for anti-polar nanoregions with increasing temperature. Therefore, the anti-polar nanoregions exhibit a fast polarization response to the applied field, causing hysteresis-free strain behavior in the studied temperature range. It is worth noting that the value of unipolar strain S_{uni} decreases in a narrow range on heating. Another advantage of electrostrictive materials is the frequency-insensitive strain behavior also because of the fast response of the anti-polar nanoregions. The unipolar strains measured at various frequencies are shown in Fig. 4(b). A frequency-insensitive electrostriction response was obtained in a wide frequency range of 0.01 Hz to 100 Hz. The evolution of S_{uni} and Q_{33} with changing temperature and frequency for the 0.76BNT–0.24NN ceramic is plotted in Fig. 4(c). Both of S_{uni} and Q_{33} values are quite stable in the temperature range from 25 °C to 250 °C and in the frequency range from 0.01 Hz to 100 Hz. Interestingly, the S_{uni} remains in a narrow range of 0.187%–0.202% in the studied temperature and frequency range, which is far superior to that of other electrostrictive ceramics such as BNT–$(Bi_{0.5}K_{0.5})TiO_3$–$(Na_{0.5}K_{0.5})NbO_3$ (BNT–BKT–NKN), 0.75NN–0.25BT and $Pb(Mg_{1/3}Nb_{2/3})O_3$ (PMN) as well as $Pb(Zr,Ti)O_3$ (PZT)-based piezoelectric ceramics, as indicated in Fig. 4(d).[7,10,12,15,32]

For ceramics with a linear dielectric response, the strain is dominated by the electrostrictive behavior and can be calculated by using $S_{33} = Q_{33}P^2 = Q_{33}\varepsilon_{33}{}^2E^2$. Q_{33} is a parameter insensitive to temperature and the phase structure. Therefore, under a fixed external electric field, the frequency and temperature stability of the electrostrictive strain should be associated directly with that of dielectric permittivity. Fig. 5(a) shows the frequency dependent dielectric permittivity ε_r at different temperatures. It can be found that the frustration of the dielectric constant is within less than ±5% of 1450 in the studied temperature and frequency range. Moreover, the dielectric response of the 0.76BNT–0.24NN ceramic is obviously larger than that of other temperature-insensitive linear dielectrics owing to the existence of the highly dynamic anti-polar nanoregions in relaxor antiferroelectrics.

To better understand the outstanding frequency stability of the polarization response, the pulsed charge–discharge speed of the $x = 0.24$ ceramic was measured. Overdamped pulsed discharge electric current–time (I–t) curves and discharge energy density ($W_D = R\int I(t)^2 dt/V$, R: total load resistor (200 Ω),

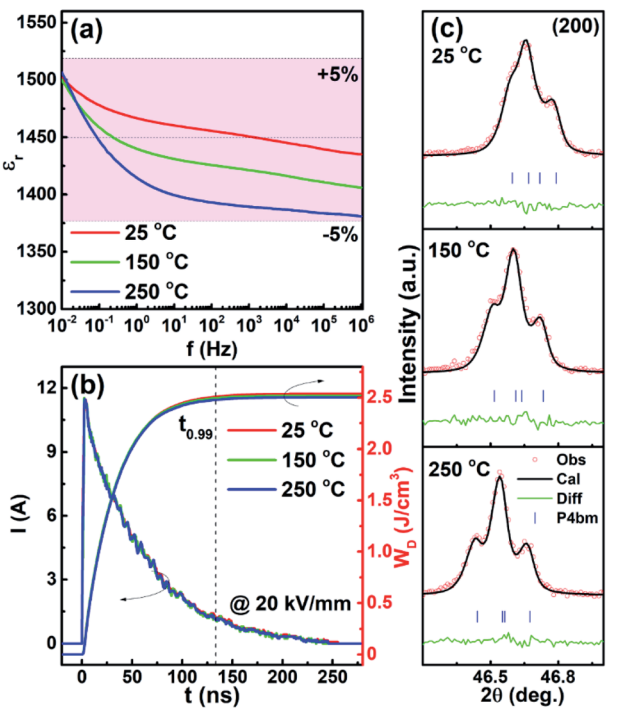

Fig. 5 (a) Temperature and frequency dependent dielectric permittivity ε_r for the 0.76BNT–0.24NN ceramic; (b) the pulsed overdamped discharge current and discharge energy density W_D as a function of time for the 0.76BNT–0.24NN ceramic at different temperatures under 20 kV mm^{-1}; (c) the Rietveld refinement results close to the (200) diffraction peaks for the 0.76BNT–0.24NN ceramic measured at different temperatures.

V: sample volume) curves measured at different temperatures are shown in Fig. 5(b). It can be found that 99% of the charge energy density ~2.5 J cm^{-3} can be released in a short discharge time ($t_{0.99}$) of ~130 ns in the studied temperature range. Such a fast discharge speed of anti-polar nanoregions is much shorter than the test period of *P*/*S*–*E* loops (>ms), thus leading to a stable hysteresis-free polarization response in the studied frequency range. To further understand the outstanding temperature stability of the electrostriction performance of the 0.76BNT–0.24NN ceramic, *in situ* XRD was employed to reveal the phase structure evolution on heating. Fig. 5(c) shows the observed, calculated, and difference profiles close to the (200) diffraction peak of the as-sintered 0.76BNT–0.24NN ceramic powders by means of the Rietveld refinement of XRD data at various temperatures using GSAS software. The existence of the *P*4*bm* phase can be well identified in the studied temperature range with a reliability factor of weighted patterns (R_{wp}), the reliability factor of patterns (R_p) and the goodness-of-fit indicator (χ^2) in the ranges of 6.8–7.1%, 5.0–5.2% and 1.2–1.3, respectively. The high activity of anti-polar nanoregions in relaxor antiferroelectrics over a wide temperature range ultimately leads to both temperature and frequency insensitive high electrostriction in the 0.76BNT–0.24NN ceramic.

Conclusions

The electrostrictive behavior of $(1-x)$BNT–xNN binary lead-free ceramics was investigated in this study. A giant hysteresis-free electrostrictive strain of ~0.20% with $Q_{33} \sim 0.030$ m^4 C^{-2} was reported in the composition of $x = 0.24$ through compositionally modulating relaxor antiferroelectric behavior. A completely linear polarization-field response was observed within a quite wide field range owing to a significantly enhanced phase transition field for antiferroelectric to ferroelectric phase transformation, for which M_{33} and Q_{33} remain constant under an electric field of higher than 20 kV mm^{-1}. Moreover, such a large electrostrictive strain features excellent stability against temperature and frequency in the range of 25–250 °C and 0.01–100 Hz, as a result of stable and high dielectric response caused by the existence of highly active anti-polar nanoregions with an ultrafast discharge (response) speed of ~130 ns. Compared with classical ferroelectric or nonpolar linear dielectric ceramics, these $(1-x)$BNT–xNN relaxor antiferroelectric materials are believed to have outstanding advantages in high-displacement and high-precision actuating or positioning applications where complex environmental conditions exist.

Conflicts of interest

There are no conflicts of interest to declare.

Acknowledgements

This work was financially supported by the National Natural Science Foundation of China (Grant No. 51472069 and U19A2087) and the China Postdoctoral Science Foundation (Grant No. 2018M642998).

References

1 B. Narayan, J. S. Malhotra, R. Pandey, K. Yaddanapudi, P. Nukala, B. Dkhil, A. Senyshyn and R. Ranjan, *Nat. Mater.*, 2018, **17**, 427–431.
2 C. Ang and Z. Yu, *Adv. Mater.*, 2006, **18**, 103–106.
3 H. Qi, R. Z. Zuo, J. Fu and M. X. Dou, *Appl. Phys. Lett.*, 2017, **110**, 112903.
4 S. T. Zhang, A. B. Kounga, W. Jo, C. Jamin, K. Seifert, T. Granzow and D. Damjanovic, *Adv. Mater.*, 2009, **21**, 4716–4720.
5 J. Yin, G. Liu, C. L. Zhao, Y. L. Huang, Z. T. Li, X. M. Zhang, K. Wang and J. G. Wu, *J. Mater. Chem. A*, 2019, **7**, 13658–13670.
6 F. Li, L. Jin, Z. Xu and S. J. Zhang, *Appl. Phys. Rev.*, 2014, **1**, 011103.
7 K. Uchino, S. Nomura, L. E. Cross, S. J. Jang and R. E. Newnham, *J. Appl. Phys.*, 1980, **51**, 1142.
8 L. E. Cross, S. J. Jang, R. E. Newnham, S. Nomura and K. Uchino, *Ferroelectrics*, 1980, **23**, 187–191.
9 S. J. Jang, K. Uchino, S. Nomura and L. E. Cross, *Ferroelectrics*, 1980, **27**, 31–34.
10 J. G. Hao, Z. J. Xu, R. Q. Chu, W. Li and J. Du, *J. Mater. Sci.*, 2015, **50**, 5328–5336.
11 H. S. Han, W. Jo, J. K. Kang, C. W. Ahn, I. W. Kim, K. K. Ahn and J. S. Lee, *J. Appl. Phys.*, 2013, **113**, 154102.
12 R. Z. Zuo, H. Qi, J. Fu, J. F. Li, M. Shi and Y. D. Xu, *Appl. Phys. Lett.*, 2016, **108**, 232904.
13 F. Li, L. Jin and R. P. Guo, *Appl. Phys. Lett.*, 2014, **105**, 232903.
14 R. E. Newnham, *Properties of Materials: Anisotropy, Symmetry, Structure*, Oxford University Press, 2005.
15 Y. Saito, H. Takao, T. Tani, T. Nonoyama, K. Takatori, T. Homma, T. Nagaya and M. Nakamura, *Nature*, 2004, **432**, 84–87.
16 X. Lu, L. Hou, L. Jin, D. W. Wang, Q. Y. Hu, D. O. Alikin, A. P. Turygin, L. Wang, L. Zhang and X. Y. Wei, *J. Eur. Ceram. Soc.*, 2018, **38**, 3127–3135.
17 W. J. Wu, J. Ma, N. N. Wang, C. Y. Shi, K. Chen, Y. L. Zhu, M. Chen and B. Wu, *J. Alloys Compd.*, 2020, **814**, 152240.
18 Y. L. Huang, C. L. Zhao, J. Yin, X. Lv, J. Ma and J. G. Wu, *J. Mater. Chem. A*, 2019, **7**, 17366–17375.
19 R. Korobko, A. Patlolla, A. Kossoy, E. Wachtel, H. L. Tuller, A. I. Frenkel and I. Lubomirsky, *Adv. Mater.*, 2012, **24**, 5857–5861.
20 N. Yavo, A. D. Smith, O. Yeheskel, S. R. Cohen, R. Korobko, E. Wachtel, P. R. Slater and I. Lubomirsky, *Adv. Funct. Mater.*, 2016, **26**, 1138–1142.
21 K. Uchino, L. E. Cross, R. E. Newnham and S. Nomura, *J. Appl. Phys.*, 1981, **52**, 1455.
22 H. Qi and R. Z. Zuo, *J. Mater. Chem. A*, 2019, **7**, 3971–3978.
23 J. Shi, H. Q. Fan, X. Liu and A. J. Bell, *J. Am. Ceram. Soc.*, 2014, **97**, 848–853.
24 L. Shebanov, M. Kusnetsov and A. Sternberg, *J. Appl. Phys.*, 1994, **76**, 4301–4304.
25 D. Schütz, M. Deluca, W. Krauss, A. Feteira, T. Jackson and K. Reichmann, *Adv. Funct. Mater.*, 2012, **22**, 2285–2294.

26 Q. Xu, Z. Song, W. L. Tang, H. Hao, L. Zhang, M. Appiah, M. H. Cao, Z. H. Yao, Z. C. He and H. X. Liu, *J. Am. Ceram. Soc.*, 2015, **98**, 3119–3126.
27 A. Zeb, Y. Bai, T. Button and S. J. Milne, *J. Am. Ceram. Soc.*, 2014, **97**, 2479–2483.
28 G. Burns and F. H. Dacol, *Solid State Commun.*, 1983, **48**, 853–856.
29 D. S. Fu, H. Taniguchi, M. Itoh, S. Koshihara, N. Yamamoto and S. Mori, *Phys. Rev. Lett.*, 2009, **103**, 207601.
30 X. Tan, E. Aulbach, W. Jo, T. Granzow, J. Kling, M. Marsilius, H.-J. Kleebe and J. Rödel, *J. Appl. Phys.*, 2009, **106**, 044107.
31 L. Jin, W. T. Luo, R. Y. Jing, J. Qiao, J. Pang, H. L. Du, L. Zhang, Q. Y. Hu, Y. Tian, X. Y. Wei, G. Liu and Y. Yan, *Ceram. Int.*, 2019, **45**, 5518–5524.
32 H. Kungl and M. J. Hoffmann, *Acta Mater.*, 2007, **55**, 5780–5791.